Earth and Planetary Science Letters, 107 (1991) 164–172
Elsevier Science Publishers B.V., Amsterdam

[CH]

Mechanical consequences of granite emplacement during high-T, low-P metamorphism and the origin of "anticlockwise" PT paths

Mike Sandiford, Nick Martin, Shaohua Zhou and Geoff Fraser

Department of Geology, University of Adelaide, GPO Box 498, Adelaide, S.A. 5001, Australia

Received December 3, 1990; revised and accepted July 8, 1991

ABSTRACT

High-temperature (T), low-pressure (P) metamorphic belts preserve evidence of metamorphism under extremely perturbed, and hence transient, thermal regimes. PT paths are commonly "anticlockwise"; that is, the maximum T was attained prior to or at the same time as the maximum P with cooling at near constant or increasing P, and, in many terrains, peak metamorphic temperatures prevailed during convergent deformation. Using a simple coupled thermal–mechanical model that assumes a strongly temperature-dependent rheology for the continental lithosphere we show that the coincidence of metamorphism with convergent deformation in high-T, low-P terrains may reflect the thermal weakening attendant with rapid advective movement of heat within the lithosphere via granite magma ascent. The model shows that the magnitude of the thermal weakening effect is sensitive to the critical temperature for granite segregation, T_{crit}, the depth of emplacement of the magmas and, most importantly, the granite forming mechanism. During the prograde cycle material points attain maximum temperatures during a transient (< 3 Ma) high strain rate pulse with $\dot{\epsilon}$ up to $\sim 10^{-14}$ s^{-1}. At levels near the site of granite emplacement, the attainment of maximum pressures follows peak temperatures with rapid cooling paths that are close to isobaric or involve slight compression.

1. Introduction

Metamorphism within convergent orogenic belts is often interpreted as the direct consequence of the deformation and subsequent erosion of the lithosphere with the form of the P–T paths followed by individual rocks reflecting the rate and geometry of material advection. Importantly, models of convergent orogens that assume this simplistic dependence of metamorphism on deformation and erosion predict "clockwise" PT paths with maximum temperatures (T_{max}) attained after P_{max} and after the main crustal thickening deformation is terminated [1]. However, the interplay between deformation and metamorphism during orogenesis is likely to be more subtle since the way in which lithosphere deforms is sensitive to the evolving thermal structure of the orogen. This is particularly the case in high-T, low-P metamorphic terrains where metamorphism and deformation is often spatially and temporally related to granite emplacement [2,3] and which commonly exhibit "anticlockwise" PT paths with T_{max} attained at the same time or prior to P_{max} during the main crustal thickening deformation [4,5]. The thermal structure of such terrains is necessarily the result of considerable magmatic heat advection raising the possibility that the observed deformation is a consequence of the thermal weakening induced by the ascent of magmas within the lithosphere [e.g. 3,4]. This possibility is supported by the observation that, for thermal structures appropriate to the generation of granitic melts at deep crustal levels and which therefore allow the advection of heat to shallower levels by segregation of such melts, much of the strength of the lithosphere is concentrated in the upper crust at levels appropriate to low P metamorphism [e.g. 6]. In this paper we investigate the thermal weakening effect of granite emplacement in orogens which may generate high-T, low-P metamorphism using a simple thermo-mechanical model, and consider the implications for the origin of "anticlockwise" PT paths.

0012-821X/91/$03.50

2. The physical model

We assume a simple "model" lithosphere consisting of two layers, a crust and a mantle lithosphere, in which the strength is controlled by quartz and olivine, respectively. At low temperatures and high strain rates the failure mechanism in both layers is modelled as frictional sliding according to Byrlee's law [7,8]:

$$\tau_s = \sigma_0 + \mu\bar{\sigma}_n \tag{1}$$

where τt_s, $\bar{\sigma}_n$, σ_0 and μ are, respectively, the shear stress and effective normal stress on the failure plane, the cohesion and the coefficient of friction. The effective normal stress is given by:

$$\bar{\sigma}_n = \sigma_n(1 - \lambda_c) \tag{2}$$

where λ_c is the ratio of fluid pore pressure to σ_n. Assuming λ_c is constant throughout the brittle crust, then for biaxial horizontal compression the maximum and minimum principle stresses are then given by [e.g. 9]:

$$\sigma_1 - \sigma_3 = -\frac{2[\sigma_0 - \nu\sigma_{zz}(1 - \lambda_c)]}{\sqrt{\mu^2 + 1} - \mu} \tag{3}$$

At higher temperatures, the failure mechanism for horizontal compression is modelled as: (1) power law creep in the crust for all $(\sigma_1 - \sigma_3)$ and in the mantle for $(\sigma_1 - \sigma_3) < 200$ MPa (e.g. [8]):

$$\sigma_1 - \sigma_3 = \left(\frac{\dot{\epsilon}}{A_p}\right)^{1/n} \exp\left(\frac{Q_p}{nRT}\right) \tag{4}$$

where A_p is a material constant, n is the power law exponent, Q_p is the activation energy, R is the gas constant and $\dot{\epsilon}$ is the strain rate; or (2) Dorn law creep in the mantle for $(\sigma_1 - \sigma_3) \geqslant 200$ MPa (e.g. [8]):

$$\sigma_1 - \sigma_3 = \sigma_d\left(1 - \sqrt{\frac{RT}{Q_d}\ln\left(\frac{\dot{\epsilon}_d}{\dot{\epsilon}}\right)}\right) \tag{5}$$

TABLE 1

Values of parameters used in calculations

z_{c0}	initial crustal thickness	35 km	
z_{l0}	initial lithospheric thickness	100 km	
T_l	temperature at base of lithosphere	1280°C	
T_s	temperature at surface of lithosphere	0°C	
ρ	density at T_l	2800 kg m^{-3}	(crust)
		3300 kg m^{-3}	(mantle)
α	coefficient of thermal expansion	3×10^{-5} K^{-1}	
k	thermal conductivity	3 W m^{-1} K^{-1}	
κ	thermal diffusivity	1×10^{-6} m^2 s^{-1}	
λ_c	ratio of pore pressure to s_{zz}	0–0.4	(crust)
μ	coefficient of friction	0.85	($\sigma_n < 200$ MPa) [a]
		0.6	($\sigma_n \geqslant 200$ MPa) [a]
c	cohesion	0	($\sigma_n < 200$ MPa) [a]
		60 MPa	($\sigma_n \geqslant 200$ MPa) [a]
A_p	pre-exponential constant for	5×10^{-6} s^{-1} MPa^{-3}	(quartz) [b,*]
	power law creep	7×10^{4} s^{-1} MPa^{-3}	(olivine) [b,c]
Q_p	activation energy for	1.5×10^{5} J mol^{-1}	(quartz) [d]
	power law creep	5.2×10^{5} J mol^{-1}	(olivine) [b,c]
Q_d	activation energy for Dorn law creep	5.4×10^{5} J mol^{-1}	(olivine) [b,c]
σ_d	threshold stress for Dorn law creep	5.7×10^{11} s^{-1}	(olivine) [b,c]
n	exponent for power law creep	3	

Sources of rheological constants:

[a] Byrlee [7].

[b] Brace and Kholstedt [8].

[c] Goetze [13].

[d] Jaoul et al. [14].

* Note that, following England [15] and others, the pre-exponential constant for power law creep in quartz has been corrected from the value given by Brace and Kholstedt [8].

where σ_d is the threshold stress, Q_d is the activation energy and $\dot{\epsilon}_d$ is the pre-exponential constant for Dorn law creep. The rheological parameters used in the calculations are given in Table 1.

We adopt the thin sheet approximation (e.g. [9,10]) in which components of $\dot{\epsilon}$ and horizontal velocity are independent of depth and therefore the vertically integrated strength of the lithosphere, F_l, is given by:

$$F_l = \int_0^{z_l} (\sigma_1 - \sigma_3)\, dz \tag{6}$$

and is uniquely defined only when the thermal structure and strain rate are specified. Moreover, we assume a strain rate regime appropriate to horizontal biaxial compression:

$$\sigma_1 = s_{xx}, \quad \sigma_3 = \sigma_{zz} \tag{7a}$$

$$\dot{\epsilon}_{zz} = -\dot{\epsilon}_{xx} = \dot{\epsilon} \tag{7b}$$

$$\dot{\epsilon}_{yy} = 0 \tag{7c}$$

Thus eq. 6 is equivalent to:

$$F_l = \int_0^{z_l} (\sigma_{xx} - \sigma_{zz})\, dz \tag{8}$$

Initially, the lithosphere is assumed in thermal equilibrium with normal thickness continental crust, $z_{c0} = 35$ km, and lithosphere, $z_{l0} = 100$ km (we term the lithosphere at the initial conditions the reference lithosphere). We parameterize the thermal state of the lithosphere in terms of the initial surface heat flow, q_{s0}, assuming that heat production occurs only in the crust where it is homogeneously distributed with depth. The shear strength of our reference lithosphere as a function q_{s0} and $\dot{\epsilon}$ is shown in Fig. 1.

We consider the reference lithosphere is subject to the application of a driving force for convergent deformation, F_{d0} at time 0, to generate a theoretical limiting crustal thickening factor of $f_c \sim 1.6$ that seems appropriate to the generation of high-T, low-P metamorphic belts (see discussion by Sandiford and Powell, [4]). We assume that the mantle lithosphere behaves in a way that maintains a constant average heat flux across the mantle during convergent deformation. As described by Sandiford and Powell [11] the rate of gain of potential energy with crustal thickening is sensitive to the mantle lithospheric response. The upper limit to crustal thickening of $f_{c,lim} \sim 1.6$ (where $f_{c,lim}$ is defined by F_b ($f_c = f_{c,lim}$) = F_{d0}) is achieved by imposing a driving force of $F_d = 5 \times 10^{12}$ N m^{-1}. It is important to note that F_{d0} does not represent the absolute magnitude of the driving force transmitted from the ocean lithosphere to the continents (for example, from the "plate tectonic" forces of ridge push and slab pull) since we have made no assumptions about the potential

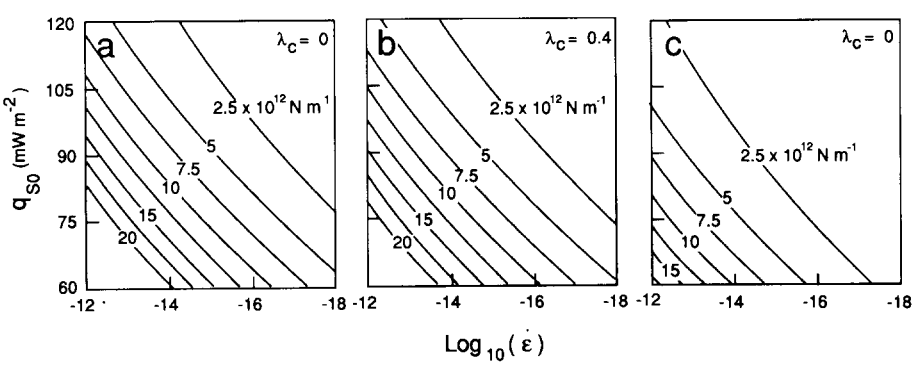

Fig. 1. a. The strength of the reference lithosphere ($z_{l0} = 100$ km, $z_{c0} = 35$ km) per unit length of orogen as a function of strain rate and the thermal state (parameterized here in terms of the initial surface heat flow, q_{s0}) for the parameter range outlined in Table 1 with $\lambda = 0$. b. As for a, but with $\lambda_c = 0.4$, and indicating that the value of the pore fluid pressure in the crust has only a small effect on the strength of the total lithosphere. c. As for a, but with activation energies for creep 10% less than the values of the parameter range outlined in Table 1, with $\lambda_c = 0$, and indicating that small uncertainties in the value of the rheological constants may have a profound influence on the strength of the lithosphere [9]. In order to attain significant strain rates (i.e., $\dot{\epsilon} > 10^{-16}$ s^{-1} for the parameter range listed in Table 1 subject to a driving force appropriate to limiting crustal thickening strains of $f_c \sim 1.6$, i.e., $F_{d0} = 4.5$ to 5×10^{12} N m^{-1}) we use initial thermal regimes characterised by surface heat flows of $q_{s0} > 80$ mW m^{-2}. Contour intervals are $F_l = 2.5 \times 10^{12}$ N m^{-1}.

energy of our reference lithosphere with respect to, for example, the mid-ocean ridges. Rather, F_{d0} represents the component of such "plate tectonic" driving forces transmitted through our reference lithosphere. Thus in the models presented here the reference lithosphere can be considered as a stress guide transmitting a force, of magnitude F_{d0}, across the boundaries of the deforming zone.

The specification of an initial driving force and thermal structure provides a sufficient set of conditions to enable the evaluation of the strain rates in the deforming lithosphere according to the force balance:

$$F_{ed} = (F_{d0} - F_b) = F_l \tag{9}$$

where F_{ed} is the effective driving force given by the difference between the initial driving force F_{d0} and the buoyancy forces, F_b, that arise as a consequence of the deformation. The buoyancy force is measured relative to the reference lithosphere:

$$F_b = \int_0^{z_l} (\sigma_{zz,d} - \sigma_{zz,r}) dz \tag{10}$$

where $\sigma_{zz,d}$ and $\sigma_{zz,r}$ are the vertical stresses at depth z in the deformed and reference lithospheres, respectively, and, assuming local isostatic compensation, is approximated by:

$$\frac{F_b}{g\rho_l z_c^2} = \delta \frac{1-\delta}{2}(f_c^2 - 1) - \frac{\alpha T_l}{6\psi^2}\left[f_l^2 - 1 - 3(1-\delta)(f_c f_l - 1)\right] - \frac{\alpha^2 T_l^2}{8\psi^2}(f_l^2 - 1) \tag{11}$$

where f_c and f_l are the crustal and lithospheric thickening factors, ψ is the ratio z_{c0}/z_{l0}, δ is the ratio, R_c/R_m, of crustal and mantle densities, and α is the coefficient of thermal expansion (note that eq. 11 is the corrected version of eq. 2 from Sandiford and Powell [11]).

For temperature and depth independent thermal diffusivity, κ, the thermal structure of the deforming lithospheric column is given by:

$$\frac{DT}{Dt} = \kappa \frac{D^2 T}{Dz^2} + \frac{H_{(z)}}{c_p \rho} \tag{12}$$

where $H_{(z)}$ is the volumetric heat production at depth z, c_p is the heat capacity, ρ is the density. Equation 12 is approximated using a Crank-Nicolson finite difference scheme modified to allow variable spaced grid points (a modification that reduces the scheme to 1st-order accuracy in space). In the one-dimensional models presented here intrusion is effectively that of an infinite sill. We do not explicitly incorporate the latent heat of crystallization. However, we note that the thermal evolution around a sill of thickness z with no latent heat liberated during crystallisation, approximates the evolution of a sill of notional thickness z', liberating latent heat, L:

$$z' = z\left(\frac{T_{dif} c_p}{T_{dif} c_p + L}\right) \tag{13}$$

where T_{dif} is the temperature difference between the sill and the country rock, c_p is the heat capacity of the sill. Typical values of $L \sim 3 \times 10^5$ J kg^{-1}, $c_p \sim 1 \times 10^3$ J kg^{-1} K^{-1}, and, in the experiments below, $T_{dif} \sim 500$ K, give:

$$z' \approx \frac{5}{8} z$$

Importantly, the results outlined below show that the mechanical evolution of our model lithosphere is not particularly sensitive to intrusion thickness and therefore to total heat transported by magmatism. Thus any small errors introduced by this approximation are not regarded as significant.

For driving forces appropriate to $f_{c,lim} \sim 1.6$, that is $F_{d0} \sim 5 \times 10^{12}$ N m^{-1}, initial heat flows of the order of $q_{s0} > 75$ mW m^{-2} are needed to generate geologically significant strain rates ($\dot{\epsilon} > 10^{-16}$ s^{-1}, Fig. 1). Such high heat flows may be reasonable if convergent deformation is initially localised at a rifted margin or a thermally perturbed margin developed in conjunction with ocean basin closure. However, it is important to realise the limitations inherent in the type of modelling undertaken here since, for the thermal regimes and strain rates appropriate to continental deformation, the strength of the lithosphere is very sensitive to the magnitude of the empirically determined rheological constants. For example, Sonder and England [9] show that a 10% decrease in the activation energies for creep has the equivalent effect on lithospheric strength as decreasing Moho temperature by ~ 100°C. In terms of the parameterization adopted here, decreasing activa-

tion energies for creep by 10% has the equivalent effect on lithospheric strength as decreasing q_{s0} by 25–30 mW m^{-2} (Fig. 1c), and yields geologically significant strain rates ($\dot{\epsilon} > 10^{-16}$ s^{-1}) in a normal continental heat flow regime (60 mW m^{-2}) for $F_{d0} \sim 5 \times 10^{12}$ N m^{-1}. In comparison with the effect of uncertainties in the rheological constants on lithospheric strength, the effect of pore pressure in the crust (see eq. 3) is relatively small, with Fig. 1b showing that an increase in λ_c from 0 to 0.4 has an equivalent effect on strength as increasing the heat flow by ~ 5 mW m^2.

In as much as the rheological constants are not precisely defined and the assumed compositional structure is highly idealised, the parameter range adopted in the models presented here (Table 1) provides, at best, a simple model enabling the evaluation of the transient thermal effects in a lithosphere which is characterised by distinct strength maxima at a number of discrete levels. We emphasize, that the principal aim of the model is to provide an insight into the behaviour of such a lithosphere subject to an externally applied stress field when a transient thermal process affects the rheology in one or more of these strength-controlling levels.

3. Results

Figures 3–8 illustrate the results of model runs for various granite emplacement geometries. These results are discussed below beginning with an outline of the general mechanical behaviour of our model lithosphere in the absence of magmatic advection of heat (Fig. 2). Results are presented in terms of the evolution over time of $\dot{\epsilon}$ and f_c and, in Figs. 2 and 3, the ratio of crustal strength to total lithospheric strength, designated F_c', and the ratio F_b/F_{d0}, designated F_b' (note that $F_{ed} = F_{d0}(1 - F_b')$)

3.1. *No magmatic advection of heat (Fig. 2)*

The general mechanical behaviour of the system is discussed with reference to the evolution of strain rate over time (Fig. 2a). Initial strain rates are strongly dependent on the thermal state of the lithosphere, varying from $\dot{\epsilon} \sim 10^{-15}$ s^{-1} for a $q_{s0} = 90$ mW m^{-2} to $\dot{\epsilon} \sim 10^{-16}$ s^{-1} for $q_{s0} = 80$ mW m^{-2}. With small finite strain increments, the vertical advection of material within the deforming lithosphere with little attendant heating produces an increase in the strength of the crust with little

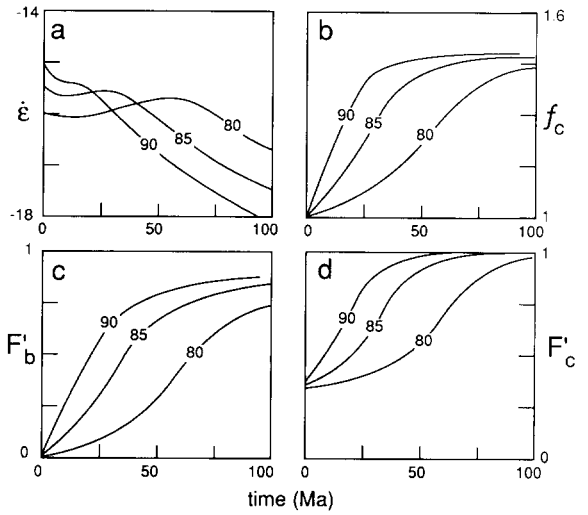

Fig. 2. Model results presented in terms of the temporal evolution of: a. $\log_{10}$ $\dot{\epsilon}$ (units of s^{-1}); b. crustal thickening strain, f_c; c. F_b', the ratio of buoyancy forces to initial driving forces; d. F_c', the ratio of the strength of the crust, F_c, to the strength of the lithosphere, F_l. Results are presented for three different initial thermal configurations appropriate to initial surface heat flows of 80, 85 and 90 mW m^{-2} and assume $\lambda_c = 0.4$. Run parameters are as indicated in Table 1 with $F_{d0} = 5 \times 10^{12}$ N m^{-1}. No granite generation occurs in these models.

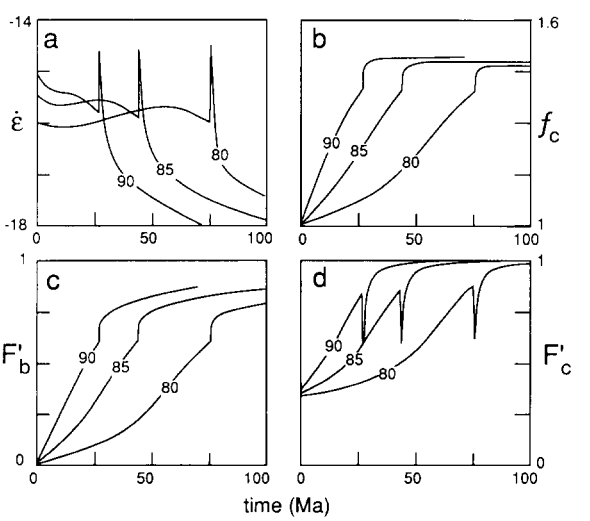

Fig. 3. Same as for Fig. 2, but with granite generation when Moho achieves temperatures of $T_{crit} = 800$°C with intrusion thickness $z = 2.3$ km ($z' = -1.5$ km) emplaced at 10 km depth.

change in the strength of the mantle lithosphere (Fig. 2d) and hence leads to declining strain rates. With increasing finite strain and time, material points begin to heat in response to the increasing crustal heat production with the consequent reduction in lithospheric strength slowing the rate of decline in strain rates, and for some configurations leading to an increase in the strain rates. Finally, as F_b' approaches 0.3, and f_c approaches $0.5 \times f_{c,lim}$, strain rates rapidly decline in response to the reduction in F_{ed} (Fig. 2c). Strain rates diminish to insignificant values as F_b' approaches 0.8, at which time virtually all the strength of the lithosphere is concentrated in the crust, $F_c' \sim 1$.

3.2. *Granite formation as a conductive response to crustal thickening (Figs. 3–6)*

We begin by considering a granite forming mechanism involving deep crustal melting in response to the conductive heating induced by crustal thickening during on-going convergent deformation. At the time the Moho reaches the critical temperatures for generation of granites, T_{crit}, the crustal strains and strain rates are largely independent of the initial thermal configuration of the lithosphere. For $T_{crit} \sim 800°C$, approximately 80% of the lithospheric strength is concentrated in the upper crust, making the total strength of the lithosphere susceptible to the thermal weakening effects of granites lodging themselves in the upper crust (Fig. 3). However, by the time $T_{crit} \sim 800°C$ is attained, the lithosphere is sufficiently weakened that F_b' is greater than 0.6. Crustal thickening strains are therefore within a few percent of $f_{c,lim}$, placing an effective upper limit on the finite strain increments of ~ 10% associated with granite emplacement.

Figures 4–6 show that the response to granite generation due to conductive heating of the lower crust during crustal thickening is strongly dependent on the depth of emplacement (Fig. 4) and the temperature (Fig. 6) of the granite, but only weakly dependent on the thickness of the intrusion (Fig. 5). The largest thermal weakening occurs for intrusion depths $< \sim 10$ km (Figs. 4a, 4b), with the effects relatively insignificant for intrusions emplaced at depths $> \sim 15$ km (Figs. 4c, 4d). The potential for thermal weakening increases substantially with decreasing T_{crit} because the generation of granites occurs at lower F_b' ($F_b' \sim 0.45$ for $T_{crit} = 750°C$).

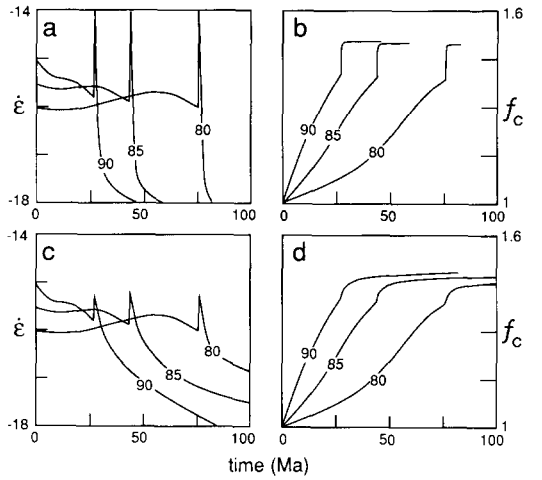

Fig. 4. In the models where granites are generated by conductive heating of the lower crust, the mechanical evolution of the system is strongly dependent on the depth of the intrusion. Figures a and b show the temporal evolution time of $\dot{\epsilon}$ and f_c for identical run parameters in Fig. 3 but for intrusion emplacement depth of 5 km, whereas c and d show the corresponding temporal evolution of $\dot{\epsilon}$ and f_c, respectively, for intrusion emplaced at a depth of 15 km.

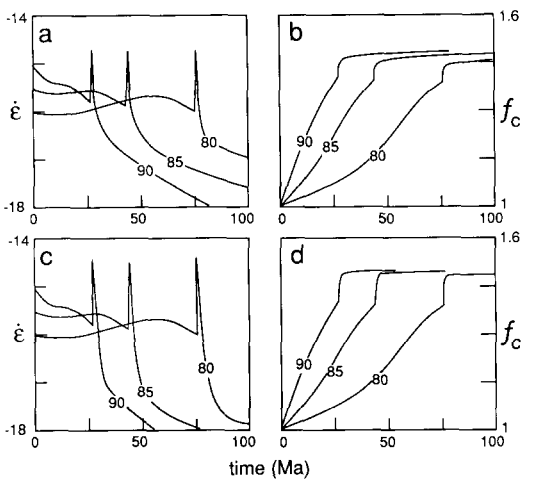

Fig. 5. In the models where granites are generated by conductive heating of the lower crust, the mechanical evolution of the system is only weakly dependent on the thickness of the intrusion. Figures a and b show the temporal evolution of $\dot{\epsilon}$ and f_c for identical run parameters in Fig. 3 but for intrusion thickness $z = 1$ km ($z' \approx 0.6$ km), whereas c and d show the corresponding temporal evolution of $\dot{\epsilon}$ and f_c, respectively, for an intrusion thickness $z = 4$ km ($z' \approx 2.5$ km).

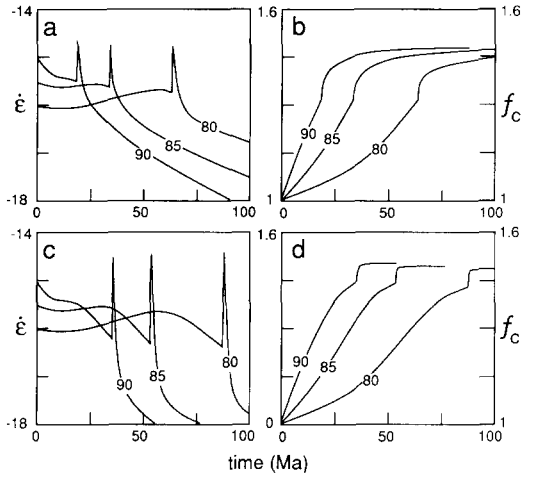

Fig. 6. In the models where granites are generated by conductive heating of the lower crust, the mechanical evolution of the system is strongly dependent on the magnitude of T_{crit}. Figures a and b show the temporal evolution $\dot{\epsilon}$ and f_c for identical run parameters in Fig. 3 but for $T_{crit} = 750°C$, whereas c and d show the corresponding temporal evolution of $\dot{\epsilon}$ and f_c, respectively, for $T_{crit} = 850°C$.

3.3. *Granite formation in response to mafic magmatic underplating (Fig. 7)*

An alternative mechanism of granite genesis in the lower crust is via roof rock melting above mafic intrusive bodies. There is no quantitative model relating deformation in convergent orogenic belts to the generation of mafic magmas in the subjacent mantle. Hence, in the models discussed below, granite genesis by accumulation of mafic melts at the Moho is considered an arbitrary

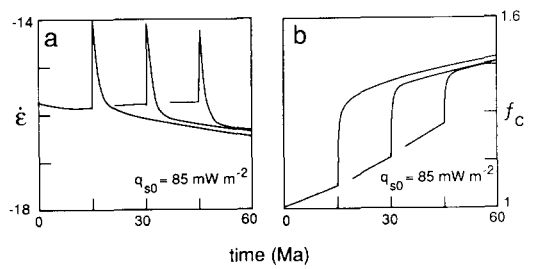

Fig. 7. Same as for Figs. 3a and 3b, with $q_{s0} = 85$ mWm^{-2}, but for granite genesis due to intrusion of mafic magma sill ($z = 3$ km) at the Moho at times 15, 30 and 45 Ma, $F_{d0} = 4.5 \times 10^{12}$ N m^{-1} and total model time of 60 Ma. The thickness of the basaltic sill emplaced at the Moho is 3 km ($z' \approx 1.8$ km) and the granite sill is 2 km ($z' \approx 1.2$ km) emplaced at 10 km depth.

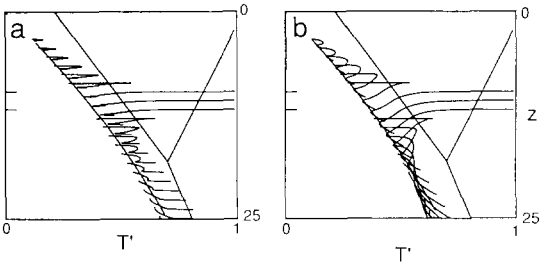

Fig. 8. a. Depth–temperature (PT) paths for the model shown in Fig. 3 with $q_{s0} = 90$ mW m^{-2}. b. Depth–temperature (PT) paths for the model shown in Fig. 7. Temperature is parameterized in terms $T' = T/T_{crit}$, with PT paths shown for the material points initially 1 km apart in the upper 25 km of the crust. For clarity, PT paths are shown only for the times after intrusion. The initial geotherm and the Al_2SiO_5 phase diagram are shown for reference.

function of time. We consider the effects for single magmatic events occurring at either 15, 30 or 45 Ma after the onset of convergent deformation (Fig. 7). Following the empirical relationship outlined by Huppert and Sparks [12] we use a mafic sill intruded at the Moho ($T_{moho} \sim 650°–700°C$) some 3 km thick ($z' \sim 1.8$ km) in order to generate a 2 km thick granite sill ($z' \sim 1.2$ km). The results clearly show that the magnitude of the thermal weakening effect is dependent on the thermal state of the lithosphere at the time of magmatic activity, with strain increments of up to 30% attendant with magmatic activity (Fig. 7b). The significantly greater thermal weakening observed in these experiments, in comparison to Fig. 3, is due to two factors: (1) a greater strength of the lithosphere at the time of the magmatic event, and (2) the thermal weakening of the mantle strength maxima due to mafic magma input.

3.4. *PT paths (Fig. 8)*

Depth–temperature (PT) paths for upper crustal rocks (< 25 km deep) are shown in Fig. 8a for model runs equivalent to Fig. 3 and in Fig. 8b for runs equivalent to Fig. 7. In Fig. 8a, PT paths for material points within a few kilometers of the granite intrusion show more or less isobaric heating, with T_{max} coincident with the transient high strain rate episode evident in Fig. 3. Maximum temperatures decay quickly away from the intrusion, and are insignificant beyond 5 km. Cooling back to the initial thermal regime occurs with only

slight compression, with residual thermal effects evident up to ~ 3 Ma after intrusion. Finally, cooling is followed by a slight increase in temperatures in response to the increased radiogenic heat production in the thickened pile. For $T_{crit} = 800°C$ and a 2 km thick sill ($z' = 1.2$ km) emplaced at 10 km depth, the peak temperatures fall within the sillimanite stability field for only a few hundred metres around the intrusion margin, while andalusite stability field is attained up to 1.8 km away. Figure 8b shows that the distribution of T_{max} with depth is comparable with Fig. 8a. However, the post-peak paths show considerably greater compression, giving rise to substantially "anticlockwise" P–T paths, in response to the greater crustal thickening increment possible when granite genesis is initiated by emplacement of mafic magmas near the Moho.

4. Discussion

The results of the simple models outlined above show that in a lithosphere subject to an external stress field appropriate to the formation of orogenic belts, the advection of granitic melts formed in the deep crust as a consequence of conductive heating during crustal thickening or the input of mafic magmas in the deep crust and/or upper lithospheric mantle may result in a dramatic, although transient (up to ~ 3 Ma), increase in the strain rate. These results are obtained for a simple lithospheric model in which strength varies with depth and is strongly temperature-dependent. The temperature-dependence allows that lithospheric strength may be transiently altered by the magmatic advection of heat. The lithosphere is assumed to have two strong zones corresponding to strength maxima in the upper part of a quartz-dominated crust and in the upper part of an olivine-dominated mantle, respectively (Fig. 1). Undoubtedly, the continental lithosphere is more complex than this two-layer analog, and probably has a number of other discontinuities in the strength–depth profile [6]. While the exact behaviour of the lithosphere subject to externally applied stress during the magmatic advection of heat will vary with the strength depth profile, the models presented here suggest that, for any strongly temperature-dependent strength profile, a significant thermal weakening may occur if the advecting magmas can lodge themselves in the "strong zones".

An important result of the models discussed here is that for granite genesis related to conductive heating of thickened crust, the magnitude of the crustal thickening strain increments associated with emplacement is restricted to less than a few percent, because, by the time lower crustal melting has taken place, the effective forces driving the deformation of the lithosphere must be significantly reduced. However, significantly larger strains may be obtained when granite magmatism is initiated by the input of mafic melts at the Moho when the Moho temperature is well below that required for crustal melting, $T_c << 750°C$. An important implication may be that any significant thermal weakening attendant with granite intrusion during high-T, low-P metamorphism occurs primarily in response to a thermal perturbation of the sub-crustal lithosphere. The magmatic advection associated with transient thermal effects will necessarily give rise to metamorphism at elevated temperatures near the sight of emplacement, with the peak metamorphic assemblages coinciding with the development of structures reflecting crustal thickening. The characteristic metamorphic imprint of the thermal weakening effect at crustal levels near the emplacement of the granite is rapid near isobaric heating during crustal thickening and subsequent cooling at constant or slightly increasing pressure; indeed such "anticlockwise" PT paths are common in many high-T, low-P metamorphic terrains found in ancient apparently convergent orogenic belts [4,5].

Acknowledgements

This research has been supported by the Australian Research Council as part of an investigation into heat and mass transfer processes in the metamorphic environment at low pressures.

References

1 P.C. England and A.B. Thompson, Pressure–temperature–time paths of regional metamorphism, 1. Heat transfer during the evolution of regions of thickened crust, J. Petrol. 25, 894–928, 1984.

2 D.R. Lux, J.J. DeYoreo, C.V. Guidotti and E.R. Decker, Role of plutonism in low-pressure metamorphic belt formation, Nature 323, 795–797, 1986.

3 E.L. Miller and P.B. Gans, Cretaceous crustal structure and metamorphism in the hinterland of the Sevier thrust belt, Western U.S. Cordillera, Geology 17, 59–6, 1989.
4 M. Sandiford and R.Powell, Some remarks on high temperature-low pressure metamorphism in convergent orogens, J. Metamorph. Geol. 9, in press, 1991.
5 R. Loosveld and M.A. Etheridge, A model for low-pressure facies metamorphism during crustal thickening, J. Metamorph. Geol. 8, 257–267, 1990.
6 A. Ord and B. Hobbs, The strength of the continental crust, Tectonophysics 158, 269–289, 1989.
7 J.D. Byrlee, Brittle–ductile transition in rocks, J. Geophys. Res. 73, 4741–4750, 1968.
8 W.F. Brace and D.L. Kholstedt, Limits on lithospheric stress imposed by laboratory experiments, J. Geophys. Res. 85, 6248–6252, 1980.
9 L.J. Sonder and P. England, Vertical averages of rheology of the continental lithosphere: relation to thin sheet parameters, Earth Planet. Sci. Lett. 77, 81–90, 1986.
10 P. Bird and K. Piper, Plane stress finite-element modes of tectonic flow in southern California, Phys. Earth Planet. Inter. 21, 158–175, 1980.
11 M. Sandiford and R. Powell, Some isostatic and thermal consequences of the vertical strain geometry in convergent orogens, Earth Planet. Sci. Lett. 98, 154–165, 1990.
12 H.E. Huppert and R.S.J. Sparks, The generation of granitic magmas by the intrusion of basalt into continental crust, J. Petrol. 29, 599–624, 1988.
13 C. Goetze, The mechanisms of creep in olivine, Phil. Trans. R. Soc. London A288, 99–119, 1978.
14 O. Jaoul, J. Tullis, A. Kronenberg, The effect of varying water contents on the creep behaviour of Heavitree Quartzite, J. Geophys. Res. 89, 4298–4312, 1984.
15 P.C. England, Diffuse deformation: length scales, rates and metamorphic evolution, Phil. Trans. R. Soc. London A321, 3–22, 1987.